Temperature and Environmentally Assisted Cracking in Low Alloy Steel

T.A. Auten, J.V. Monter

KAPL-4811
April 1995

Prepared for
The United States Department of Energy

Prepared by
Knolls Atomic Power Laboratory
P. O. Box 1072
Schenectady, New York

Contract No. DE-AC12-76-SN00052

DISCLAIMER

TABLE OF CONTENTS

TABLES

FIGURES

FIGURES (Cont'd)

TEMPERATURE AND ENVIRONMENTALLY ASSISTED CRACKING IN LOW ALLOY STEEL

T. A. Auten
The Knolls Atomic Power Laboratory
Schenectady, New York 12301-1072

J. V. Monter
The Babcock & Wilcox Company
Alliance, Ohio 44601

Abstract

Environmentally assisted cracking (EAC) can be defined as the propagation of fatigue cracks in water at rates that are anywhere from 3 to over 40 times the growth rates expected in air. For low alloy steels with sulfur contents greater than 0.0125 % by weight, EAC is considered normal behavior in the 240 to 290°C range. However, the technical literature yields mixed results for tests of low alloy steels with compositions just below this sulfur level; some reports indicate EAC while others do not. Also, several authors have reported an increased tendency toward EAC when the water temperatures were lowered. In the present work, five ASTM A 508 Class 2 forgings with ladle and check analyses that ranged from 0.010 to 0.019 wt% S were tested in high purity deaerated water in the temperature range of 93 to 260°C. At 260°C these forgings did not exhibit EAC, reinforcing earlier results for two similar forgings. This broad sampling indicates a strong resistance to EAC for this class of forging at 260°C.

On the other hand, EAC occurred consistently in the three of these forgings that were tested below 204°C, provided the test conditions (loading frequency, ΔK, and R) were high enough to produce a high baseline fatigue crack growth rate (FCGR), where the baseline FCGR is that expected in air. At 149°C, EAC occurred at test conditions that combined to yield a baseline FCGR greater than ≈2E-6 mm/s. At 204, 121, and 93°C, this "critical crack growth rate" appeared to shift to lower baseline values. The EAC that occurred at lower temperatures was a factor of 3 to 12 times higher than baseline air rates, which was not as strong as the effect for higher sulfur steels at 240 to 290°C. Also, no plateau in the growth rates occurred as it does with the higher sulfur steels. In another approach, EAC was induced at 93 and at 260°C by raising the dissolved oxygen content of the water from <10 to >15 ppb. In this case, the EAC growth rates decreased to non-EAC levels when the oxygen supply was shut off. The oxygen-related EAC occurred over a broader range of baseline growth rates than found for the growth rate driven EAC. Again, this can be rationalized by the buildup of sulfur in the crack tip water, which can be associated with the higher corrosion potential of the bulk water.

Introduction

EAC, the propagation of fatigue cracks in water at rates that are 3 to 40 times the growth rates expected in air, is considered normal behavior in the 240 to 290°C range for low alloy steels with sulfur contents greater than 0.0125 % by weight (1, 2). However, the technical literature yields mixed results for tests of low alloy steels with sulfur compositions just below this level; some reports indicate EAC while others do not (1-8). Also, several authors have reported an increased tendency toward EAC when the water temperatures were lowered from the 260 - 288°C range (1, 3, 5, 6).

The objective of the present study was to test for EAC effects under some extremes in temperature in deaerated and in oxygenated water conditions. Five ASTM A 508 Class 2 forgings with ladle analyses that ranged from 0.011 to 0.013 wt% S were tested in pH 10.2 high purity deaerated water in the temperature range of 93 to 260°C. The vendor check analyses ranged from 0.010 to 0.019 % S. EAC

was induced at 93 and at 260°C by raising the dissolved oxygen content of the water from <10 to >15 ppb.

Experimental Procedures

Test specimens were taken from the five ASTM A 508 Class II forgings designated A, C, D, E, and F in Table I, which provides the ladle chemical analyses. The ladle sulfur analyses ranged from 0.011 to 0.013 wt. %, while the product check analyses from the forging certifications ranged from 0.010 to 0.019 %, as shown in Table II under the "vendor" column. These product check analyses were typically performed on drillings taken from spent tensile specimens from the upper and lower prolongations. Using the groupings developed in the statistical review of the commercial database would put Forging A in the high sulfur category (>0.0125 %S), while Forgings C through F would be medium sulfur steels (0.005 to 0.0125%) (2). Table II also provides under the "local" column the results of LECO analyses made at KAPL on sections cut from the test specimens or from material next to the specimens. The local checks indicate that all of the forgings should be considered low sulfur, except perhaps for Forging C. The grand averages of all of the analyses are: 0.0090 %S for Forging A, 0.0126 for Forging C, 0.0103 for Forging D, 0.0088 for Forging E, and 0.0088 for Forging F. The fatigue crack propagation behavior of Forging A was reported earlier in Reference 3 and in Reference 1, in which it was designated "Heat D".

Compact tension specimens were machined to standard 2T dimensions with the thickness, B, of 51 mm (9). All the specimens were oriented for crack growth parallel to the principal tensile strain direction during forging, which is the "T-L" orientation in the fracture toughness test standard (10). These orientations were established by careful oversight of the machining process, starting with the shape and identification markings of the remnant forging materials.

All of the present tests were performed at the Alliance Research Center of the Babcock & Wilcox Company in Alliance, Ohio. The autoclave was made of AISI Type 316 stainless steel and had a 76 liter (20 gallon) capacity. The water supply was operated as a once-through system with a flow rate of 12 to 17 ml/minute. For operation as a normal low oxygen environment system, the test system was unchanged from previously reported work (11). High purity deaerated water was prepared to the desired chemistry and stored in a 200 gallon stainless steel feedwater tank with a cover gas of high purity (99.99%) hydrogen. The water composition was controlled by continuous spraying of the feedwater through a hydrogen cover gas. The hydrogen overpressure was maintained at about 28 std cc/kg H_2O, resulting in a dissolved oxygen (DO) concentration generally below 10 ppb. The purity of the water supply was controlled to keep chloride and fluoride ions to the ≈10 ppb level. The pH at room temperature was held at about 10.2 and the conductivity at 45 μS/cm.

For operation as an oxygenated water environment, the system was modified from that in Reference 3. The high purity water was prepared in the main feed water tank with a pure nitrogen cover gas; the starting water and pH were unchanged. A separate 200 gallon feedwater tank was used to prepare oxygenated water; in this case the DO content was varied by varying the oxygen content of a mixed nitrogen-oxygen cover gas. The DO in the autoclave could be controlled by changing the gas pressure in the second tank, by blending the output of the two feedwater tanks, and (as a fine adjustment) by controlling the autoclave flow rate. Oxygen sensors were placed in the feedwater inlet to the pressurizing pump and in the effluent line after the cooling coil and back-pressure relief valve. These were coupled to an Orbisphere oxygen analyzer. Unless otherwise identified, the DO values reported here were measured in the effluent water, which was piped out of the autoclave through a stainless steel tube placed within 15 mm of the specimen notch. In previous tests the outlet was located at the top of the autoclave (3, 11).

Once the specimen, displacement gage, corrosion potential coupon, and other parts of the test system had been assembled, the autoclave vessel was brought into position and sealed. The vessel was then purged with pure nitrogen gas and held for several hours. At that point, the vessel was filled with the prepared deaerated water from the feedwater tank, pressurized and heated. Testing began approximately 24 hours after the system reached the target temperature.

The free corrosion potential was measured for each test on a 25 x 25 x 3 mm section machined from each forging. This coupon was located about 15 mm from the notch tip of the specimen and was monitored by an external AgCl/KCl reference electrode. The free corrosion potential was also measured at the reference electrode with respect to the autoclave, and these values are reported here. The temperature was monitored through thermocouples placed near the specimen.

Loads were applied to the specimens through a computer-controlled servohydraulic system, which has been described in previously published work (3, 11). The load cell was mounted outside the autoclave, and a displacement transducer with encapsulated strain gages was attached to the specimen inside the autoclave. Specimen compliance was used to estimate the crack lengths and to control the tests to maintain constant values of ΔK throughout the test. Numerous constant ΔK tests were run on each specimen. Each test was continued for about 0.5 mm crack extension.

Results

The crack growth rate results are tabulated in Tables A-I through A-III in Appendix I.

Deaerated Water at 260°C

The results for the tests of Forgings C, D, E, and F at 260°C in the deaerated water environment are plotted as enlarged symbols in Figure 1. In all of these tests, the applied ΔK was 16.5 MPa$\sqrt{m}$ at a load ratio (R = minimum load/maximum load) of 0.7. The waveform for the load cycles was of the sawtooth type; the loads rose during 95% of the wavelength and fell during the remaining 5%. The crack growth rates are shown as crack tip speeds, $\dot{a}_E$, measured during the test in the water environment. These rates were calculated by dividing the measured cyclic crack growth rate in mm/cycle by the rise time per cycle (2):

$$\dot{a}_E = \frac{da}{dN \cdot t_R} \tag{1}$$

The $\dot{a}_E$ are compared with baseline growth rates, $\dot{a}_B$, which are those expected for tests in air (2). The baseline growth rates are calculated from a best-fit curve through a large database of fatigue crack growth rates for low alloy steels in air at 288°C divided by the rise time:

$$\dot{a}_B = \frac{7.87 \cdot 10^{-8}}{t_R}\left(\frac{\Delta K}{2.88-R}\right)^{3.07} \tag{2}$$

where $\dot{a}_B$ is in mm/sec and ΔK is in Mpa$\sqrt{m}$.

If there were no effect of the environment, then a plot of the $\dot{a}_E$ data against $\dot{a}_B$ would result in a clustering of the points along the line $\dot{a}_E = \dot{a}_B$. A mean line for crack growth in the absence of EAC has been calculated for similar steels (1):

$$\dot{a}_E = 1.69 \cdot \dot{a}_B, \tag{3}$$

which is shown in Figure 1. With one exception, the data in Figure 1 all exhibit FCGR ratios ($\dot{a}_E/\dot{a}_B$) less than 3.0, consistent with non-EAC behavior. The exception is associated with a transition from one test condition to another that was exhibited by the specimens from Forgings E and F. In both cases, the first test done on the specimen was at a baseline $\dot{a}_B$ of 2.1E-6 mm/s, which was followed by a frequency decrease from 0.05 to 0.006 Hz for the second test. When the frequency was reduced, these two specimens exhibited decreased crack growth rates, but in comparison to the new baseline rate of 2.5E-7 mm/s the measured rates were relatively high, producing an FCGR ratio of $\dot{a}_E/\dot{a}_B = 2.8$ for Forging E and 3.1 for Forging F. After some cycling (1500 cycles for Forging E and 2000 cycles for Forging F), the crack growth rates spontaneously decreased to produce $\dot{a}_E/\dot{a}_B$ levels of 1.5 and 1.2, respectively. This is shown in Figure 2, a plot of the crack length estimates vs. cycles for the second test performed on Forging E. This test was performed at t_R= 158.3 seconds and followed a test at t_R=19 s. The regression line through the data from 1500 to 13500 cycles has a slope of 1.8 in/cycle (4.6 mm/cycle). The initial 1500 cycles produced a slope of 4.3E-6 in/cycle (1.1E-4 mm/cycle). This type of transient behavior has been reported earlier for low alloy steels under similar conditions (12). The specimens from forgings C and D did not exhibit similar transitions.

Deaerated Water at Temperatures < 260°C

Tests were performed at temperatures below 260°C on two specimens from Forging A and one from Forging C. The first of these lower temperatures was 204°C for Forging C. The first test in this series started at an FCGR ratio of 5.9, which fell to 2.9 after 3000 cycles (17 hours) for another 28 hours. As shown in Figure 3, all the other tests at 204°C exhibited FCGR ratios below 2.9.

At all test temperatures below 204°C, the forgings exhibited $\dot{a}_E/\dot{a}_B$ ranging from 3 to 12, depending on the baseline crack growth rate, which was controlled via test frequency. The results at 149°C, shown in Figure 4, demonstrated that forging A exhibited a threshold for EAC behavior. Above a baseline crack growth rate of ≈2E-5 mm/s, the $\dot{a}_E/\dot{a}_B$ was typically above 3. Below that baseline level, $\dot{a}_E/\dot{a}_B$ generally fell close to the mean non-EAC (dashed) line (1).

At 121°C, Figure 5, the $\dot{a}_E/\dot{a}_B$ generally fell between 3 and 8, well above the mean non-EAC line (1). The lowest $\dot{a}_E/\dot{a}_B$ occurred on the last test in the series and suggests that a test at a lower baseline crack growth rate might have identified a threshold. However, at 2.9 cycles per hour, the tests were already very time-consuming.

At the lowest test temperature, 93°C, the $\dot{a}_E/\dot{a}_B$ ranged from 7 to 12 for Forging A and 3 to 5 for Forging C, Figure 6. The test of Forging C at the lowest baseline rate, 2.5E-7 mm/s, showed a spontaneous transition to lower growth rates, as observed in other tests near thresholds (11). However, Forging A did not exhibit any similar behavior. Forging A also exhibited significantly higher growth rates than Forging C.

Oxygenated Water Tests

The performance of the revised system for oxygen control was checked prior to the crack growth rate tests. Figure 7 shows the corrosion potential *vs.* the effluent oxygen for the trial without load cycling at 260°C. Over a 350 hour period, the system was able to meet a target level of 50 ppb with a range of +40, -20 ppb. During the actual corrosion fatigue tests, the variations were less.

The oxygenated water tests were conducted on the specimen from Forging C. At 260°C, elevated oxygen levels of 30 and 100 ppb were targeted. The measured values for the lower target level were within 30 to 55 ppb DO, and the corrosion potential rose from the normal free corrosion potential of

-680 mv to about -125 mv. At the same time the crack growth rates rose sharply to produce FCGR ratios of 16 at an applied $\dot{a}_B$ of 2.1E-6 mm/s and 64 at $\dot{a}_B$ = 2.5E-7 mm/s. At 90 to 100 ppb DO, the corrosion potential rose to about +0.030 mv, and the FCGR ratio increased to about 23 at an applied $\dot{a}_B$ of 2.1E-6 mm/s and 74 at $\dot{a}_B$ = 2.5E-7 mm/s. These FCGR results are plotted in Figure 1.

At 93°C, the addition of 35 to 50 ppb DO drove the corrosion potential from the normal free corrosion potential range of -240 to -300 mv up to about +0.060 mv. At the same time, the FCGR ratio increased to about 6 at an applied $\dot{a}_B$ of 2.1E-6 mm/s and 10 at $\dot{a}_B$ = 2.5E-7 mm/s, Figure 6. The addition of 95 to 110 ppb DO at 93°C drove the corrosion potential still higher, about +145 mv, but the FCGR ratios were virtually identical to those at 35 to 50 ppb DO.

Discussion

The corrosion potential data recorded during the trial of the oxygen control system, Figure 7, is consistent with existing data (1,13 - 15). The plot of potential *vs.* oxygen follows the form of the data obtained by Macdonald, *et al.*(13). That is, the potential rose very steeply as the oxygen content went above 10 ppb and appears to have reached a rough plateau at about 100 ppb. The position of the sigmoid curve is dependent upon the flow rate of the coolant, which might explain the offset between the Reference 13 curves and the present results (14). The position of the plateau - while not established here - depends upon having a clear definition of the hydrogen content (15). The present data at 260 and 93°C, taken with that reported at 149°C in Reference 3, do appear to be higher as the temperature is lowered, consistent with References 1 and 13.

The method of obtaining the present data should produce consistent results. The nominal 15 ml/min flow rate of the effluent suggests that if the oxygen analyzer is switched on and a reading of potential is taken, the potential data should lag the oxygen analysis by at most a few minutes. The potentials obtained during the corrosion fatigue tests, such as those shown in Figure 7, were the mode values for a large number of readings taken through each test at the rate of one or two per day. Fluctuations such as those at the start of an autoclave run were not reported here. These mode values of potential plotted against the dissolved oxygen content of the water seem to follow the characteristic sigmoidal shape predicted in Reference 13, (see Figure 7).

The general result for the fatigue tests at 260°C was that the four additional medium sulfur forgings exhibited non-EAC behavior. In previous tests, similar results were obtained for two additional forgings in two different test stands (3). Also, similar results for three more forgings were obtained in Reference 1, which strongly suggests that forgings in this sulfur range tend not to exhibit EAC under these conditions over a very broad range of $\dot{a}_B$.

As noted in the results section, the only exception to non-EAC behavior at 260°C found here was associated with the transitional behavior exhibited by Forgings E and F. Transient behavior in which the crack growth rates spontaneously decreased after lowering the test frequency has been reported before for low alloy steels (12), but it is not clear why only two of the forgings tested here showed the transient.

The tests at 204°C also produced environmental growth rates that were below 3.0, except for an initial transient, which eventually decayed to non-EAC behavior. In this case, the previous test (No. 19) had been conducted at 93°C and had produced a modest elevation of the growth rates with $\dot{a}_E/\dot{a}_B$ = 3.3. However, the baseline crack growth rate was INCREASED from the preceding test, not decreased. The rest of the tests at 204°C showed no EAC; even during a return to testing at the baseline growth rate (2.1E-6 mm/s) at which the original transient occurred, Figure 3.

The tests at 149°C in Figure 4 provide strong support for the existence of a threshold for the medium sulfur steels. This threshold is a value of the baseline crack growth rate, $\dot{a}_B$, above which modest EAC occurs. To illustrate this more clearly, the individual data points for specimen 6B have been numbered in their order of occurrence in this figure. Tests 1, 2, 3, 4, and 6 all were on the upper side of the threshold, while tests 5 and 7 were on the lower side. When combined with the results for specimen CA5-10 (for the sake of clarity, these tests are not numbered) and with the results from Reference 3, this sequence indicates that a threshold for these steels occurs at ≈2.1E-6 mm/s. Note that there was little hysteresis in the threshold as the baseline $\dot{a}_B$ was raised or lowered.

The threshold for the 149°C tests is very similar to one discussed in Reference 1 for an A302-B steel with 0.019 %S, which is shown in Figure 4. The threshold for the higher sulfur steel occurred at a lower baseline $\dot{a}_B$, roughly 5E-7 mm/s. The threshold provides additional support for the model that proposes that EAC in low alloy steels requires the buildup of sulfur in the crack tip water to a critical level (16, 17). The supply of sulfur comes from the dissolution of MnS inclusions in the steel that have been exposed to the water by the advance of the fatigue crack tip. The sulfur ions in the crack tip can migrate out into the bulk water by diffusion, by electrochemically-aided diffusion, and by convection. The latter may be aided by high flow rates of the test water or by the mechanical "pumping" of crack in fatigue. If the mechanical driving force for crack growth is low enough, the supply of sulfur will be slowed and the sulfur ions can migrate out of the crack tip at a rate high enough to drop the sulfur concentration below the critical level, shutting off EAC. On the other hand, a modest EAC can be induced by increasing the baseline crack growth rate, which increases the sulfur supply.

Although the growth rates at 121 and 93°C indicated that EAC behavior dominated at all tested levels of $\dot{a}_B$, possible threshold behavior was suggested by the spontaneous decreases in $\dot{a}_E$ that occurred during the lowest baseline $\dot{a}_B$ test of Forging C. The sequence numbers for Forging C in Figure 6 show that the last test (No. 6) on this specimen was conducted at an $\dot{a}_B$ of 2.5E-7 mm/s, producing an initial growth rate of 1.1E-6 mm/s. However, after 1550 cycles or 72 hours, the growth rates fell to 8.3E-7 mm/s (datum No. 7). Taken together, the results at the various temperatures suggest that the threshold for EAC shifts downward with temperature, as indicated in Figure 8; but the evidence for the threshold at the lower temperatures is thin.

The fatigue tests in oxygenated water reproduced the strong effects seen earlier (3, 17, 18). However, the effect on crack growth rates was significantly greater at 260°C than at 93°C. Although the corrosion potentials measured in the oxygenated water at 149°C were higher than those at 260°C, the differences in potential between oxygenated and deaerated conditions were greater at 260°C. The deaerated water potential at the higher temperature is about -680 mv, based on the behavior in the tests of all forgings. At the nominal 40 ppb DO level, the potential of -115 mv yields a difference of 565 mv, while at 100 ppb DO level the potential of about +20 mv produces a potential difference of 700 mv. At 93°C, the deaerated water potential is about -260 mv. At the nominal 45 ppb DO level, the potential of +60 mv yields a difference of 320 mv, while at the 100 ppb DO level the potential of about +145 mv produces a potential difference of 405 mv. Since the crack tip region remains relatively deaerated as the bulk water oxygen increases (16, 19, 20), these differences in potential between the oxygenated and deaerated conditions suggest that the crack tip has a greater potential difference with respect to the oxygenated bulk water at 260°C than it does at 93°C. This potential difference tends to resist the migration of the sulfur ions from the crack tip, favoring EAC.

The effect of oxygen does not appear to be a transient response; that is, if oxygen is present in the water, it does not require an incubation period to have an effect. If the oxygen mechanism involved migration of oxygen ions into the crack tip, some lag time would be expected. A pre-exposure of the specimen from Forging C to oxygenated water at 66°C under constant load was performed and should

have permitted this to occur, but subsequent tests at 260°C showed no evidence of the prior oxygen exposure.

Summary and Conclusions

In summary, four low alloy steel forgings with nominally medium sulfur contents exhibited non-environmentally assisted cracking at 260°C in deaerated pH 10.2 water. When coupled with data from two earlier publications (1, 3), the present results suggest that A508 Class 2 forgings in this sulfur range tend not to exhibit EAC under these conditions. However, modest EAC behavior was induced at 149°C by increasing the test conditions (ΔK, R, loading frequency) to produce baseline crack tip speeds in excess of 2E-6 mm/s. At 121 and 93°C, EAC also occurred, but only weak evidence of a threshold as a function of baseline crack tip speed was seen.

Also, increasing the dissolved oxygen content of the bulk water (pH = 10.2) at both 93 and 260°C led to larger EAC effects. The addition of 30 to 55 ppb dissolved oxygen at 260°C drove the corrosion potential from the normal free corrosion potential of -680 mv to about -125 mv and increased the FCGR ratio to 16 to 64, depending upon the baseline $å_B$. The addition of 90 to 100 ppb oxygen at 260°C drove the corrosion potential to about +0.030 mv and increased the FCGR ratio to 23 to 74, depending upon the baseline $å_B$. The addition of 35 to 50 ppb oxygen at 93°C drove the corrosion potential from the normal free corrosion potential range of -240 to -300 mv up to about +0.060 mv. The addition of 95 to 110 ppb oxygen at 93°C drove the corrosion potential to about +145 mv. At both oxygen levels, the FCGR ratio increased to 6 to 10, depending upon the baseline $å_B$.

Acknowledgements

Thanks are extended to J. W. Prybylowski , C.D. Thompson, and S. Floreen of KAPL, and W. A. Van Der Sluys of the Babcock & Wilcox Research Center for their helpful discussions. We also thank several key contributors, including Ms. Carol DiPasquale, and Bruce Furbeck. This work was performed under U. S. Department of Energy Contract No. DE-AC12-76SN00052 to the Knolls Atomic Power Laboratory, which is operated by Martin Marietta.

References

1. L. A. James, J. Pressure Vessel Technology, ASME Transactions, 117 (May) (1994) pp. 122-127.
2. E. A. Eason et al., Nuclear Engineering and Design, 115(1)(1989), pp. 23-30.
3. T. A. Auten, S. Z. Hayden, and R. H. Emanuelson, Proceedings of the Sixth International Symposium on Environmental Degradation of Materials in Nuclear Power Systems - Water Reactors, San Diego, California, TMS/AIME (1993), pp. 35-41.
4. W. H. Cullen, K. Törrönen, and M. Kemppainen, "Effects of Temperature on Fatigue Crack Growth of A 508-2 Steel in LWR Environment", NUREG/CR-3230, April, 1983.
5. J. D. Atkinson and Z. Chen, Proceedings of the Sixth International Symposium on Environmental Degradation of Materials in Nuclear Power Systems - Water Reactors, San Diego, California, TMS/AIME (1993), pp. 29-34.
6. D. R. Tice, D. Worswick, P. Hurst, and H. Fairbrother, Proceedings of the Sixth International Symposium on Environmental Degradation of Materials in Nuclear Power Systems - Water Reactors, San Diego, California, TMS/AIME (1993), pp. 19-27.
7. W. A. Logsdon, P. K. Liaw, and J. A. Begley, Fracture Mechanics, 19th Symposium, ASTM STP 969, American Society for Testing and materials, Philadelphia, 1988, pp. 830-867.
8. P. K. Liaw, W. A. Logsdon, and J. A. Begley, Metallurgical Transactions A, Vol. 20A, October, 1989, pp. 2069-2085.
9. "Standard Test Method for Measurement of Fatigue Crack Rates", ASTM Standard E 647-88a.
10. "Standard Test Method for Plane-Strain Fracture Toughness of Metallic Materials", ASTM Standard E 399-83.
11. W. A. Van Der Sluys and R. H. Emanuelson, Environmentally Assisted Cracking: Science and Engineering, ASTM STP 1049, (1990) pp. 117-135.
12. W. A. Van Der Sluys, E. D. Eason, and J. D. Gilman, Proceedings of the Fourth International Symposium on Environmental Degradation of Materials in Nuclear Power Systems - Water Reactors, NACE, Houston, Texas (1990), pp. 37-62.
13. D. D. Macdonald, Z. Smialowska, S.P. Pednekar, I. Mizumo, and H. Choi, EPRI Progress Report T IIS-S (1980).

14. D. D. Macdonald, Corrosion, Vol. 48 (No.1), 1993, pp. 8-16.
15. A. Turnbull and M. Psiala-Dombrowski, Corrosion Science, Vol. 33 (No.12) 1992, pp. 1925-1966.
16. P. Combrade, M. Foucault, and G. Slama, Proceedings of the Third International Symposium on Environmental Degradation of Materials in Nuclear Power Systems - Water Reactors, TMS/AIME, Traverse city, Michigan, (1988), pp. 269-276.
17. P. L. Andresen and L. M. Young, "Crack Tip Chemistry and Growth Rate Measurement in Low Alloy Steel in High Temperature Water", Report 94CRD024, GE Research & Development Center, February, 1994.
18. J. D. Atkinson, Proceedings of the Fourth International Symposium on Environmental Degradation of Materials in Nuclear Power Systems - Water Reactors, NACE, Houston, Texas (1990), pp. 64-76.
19. F. P. Ford and P. L. Andresen, Parkins Symposium on Fundamental Aspects of Stress Corrosion Cracking, TMS/AIME, 1992, pp. 43-67.
20. G. Gaebetta and G. Buzzanca, Proc. 2nd Int. Atomic Energy Agency Specialists Meeting on Subcritical Crack Growth 1, 2, Sendai, Japan (May, 1985), NUREG/CP0067, Vol. 2, pp. 201-218.

Table I. Ladle Analyses for the Test Forgings

Forging	C	Mn	P	S	Si	Ni	Cr	V	Mo
A	0.22	0.60	0.008	0.013	0.26	0.70	0.38	0.01	0.62
C	0.22	0.63	0.010	0.012	0.27	0.73	0.35	0.01	0.59
D	0.22	0.62	0.013	0.011	0.25	0.69	0.38	0.01	0.60
E	0.20	0.66	0.011	0.012	0.24	0.69	0.34	<0.01	0.59
F	0.20	0.75	0.007	0.011	0.22	0.85	0.38	0.035	0.63

Table II. Detailed Sulfur Analyses for the Test Forgings

Forging Number	Specimen Number	<-Check Sulfur Analyses-> Vendor wt.%	Local (at KAPL) wt.%	<-Tensile Data-> Temp. °C	Yield Mpa	Tensile Mpa
A	6B and	0.013	0.0067 to 0.0086	260	334	512
	CA5-10	0.012	Average =0.0076	127	335	500
C	CA5-50	0.014	0.012, 0.013	260	415	594
		0.016	0.011, 0.010	93	450	598
D	CA5-51	0.019	0.009, 0.007	260	443	608
		0.010	0.007, 0.009	93	437	579
E	CA5-70	0.013	0.006, 0.007	260	416	558
		0.011	0.006, 0.007	93	427	556
F	CA5-80	0.012	0.010, 0.009	260	498	640
		0.012	0.009, 0.009	93	518	641

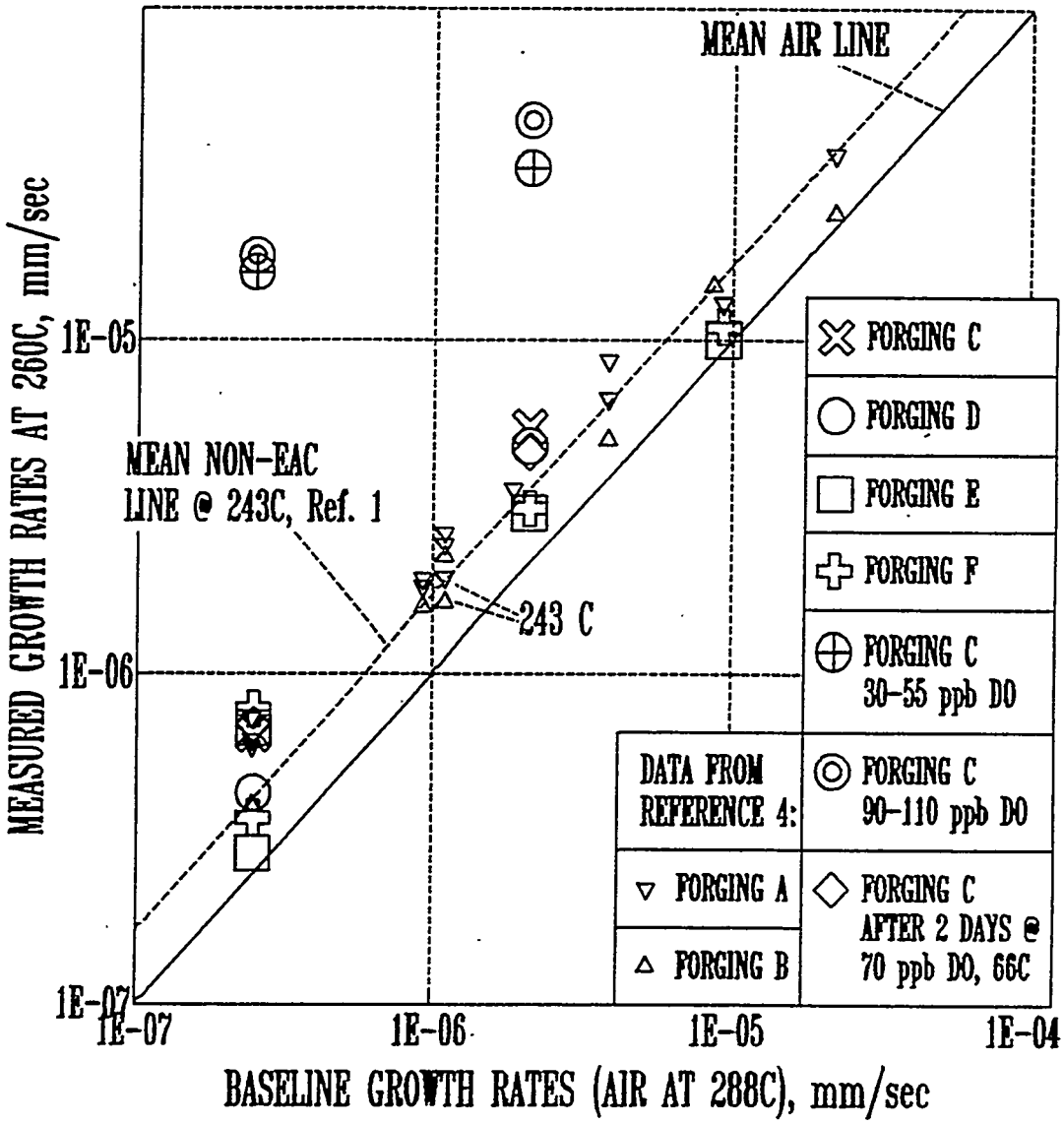

Figure 1. Environmental Fatigue Crack Growth Rates at 260°C Plotted Against Baseline Air Crack Growth Rates. The present data are shown as enlarged symbols.

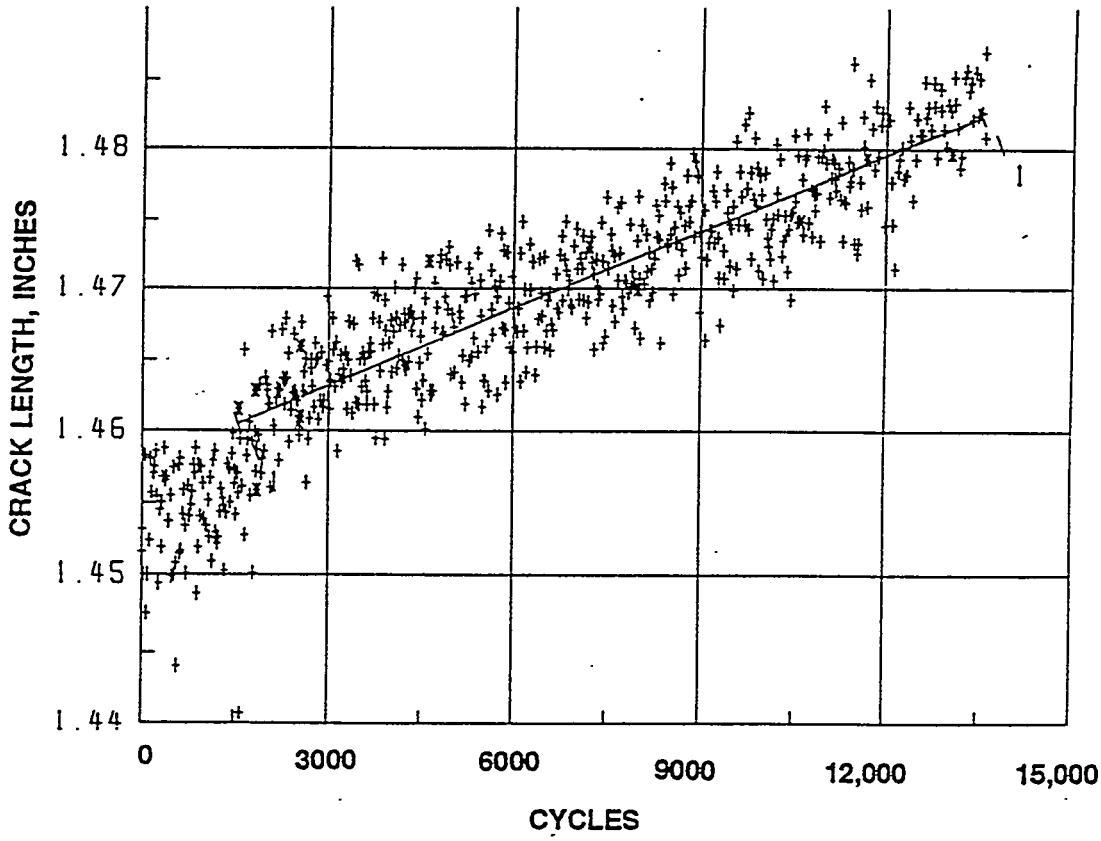

Figure 2. Plot of Crack Length vs. Cycles for the Second Test of the Specimen Machined from Forging E. This test was run under low oxygen conditions at 260 C, ΔK = 16.5 Mpa$\sqrt{m}$, R=0.7 and t_R = 158.3s.

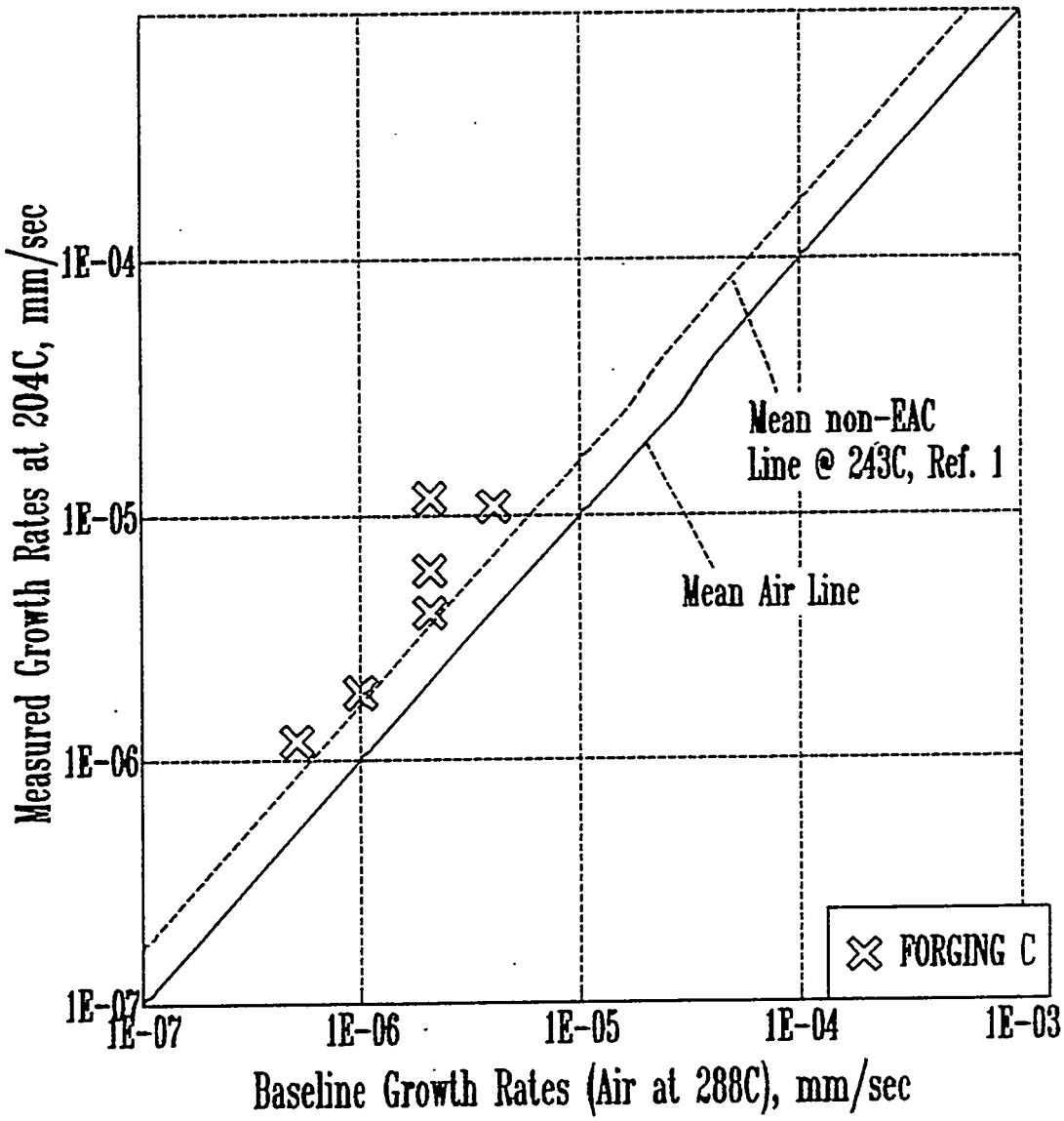

Figure 3. Environmental Fatigue Growth Rates for Forging C at 204°C Plotted Against Baseline Crack Growth Rates.

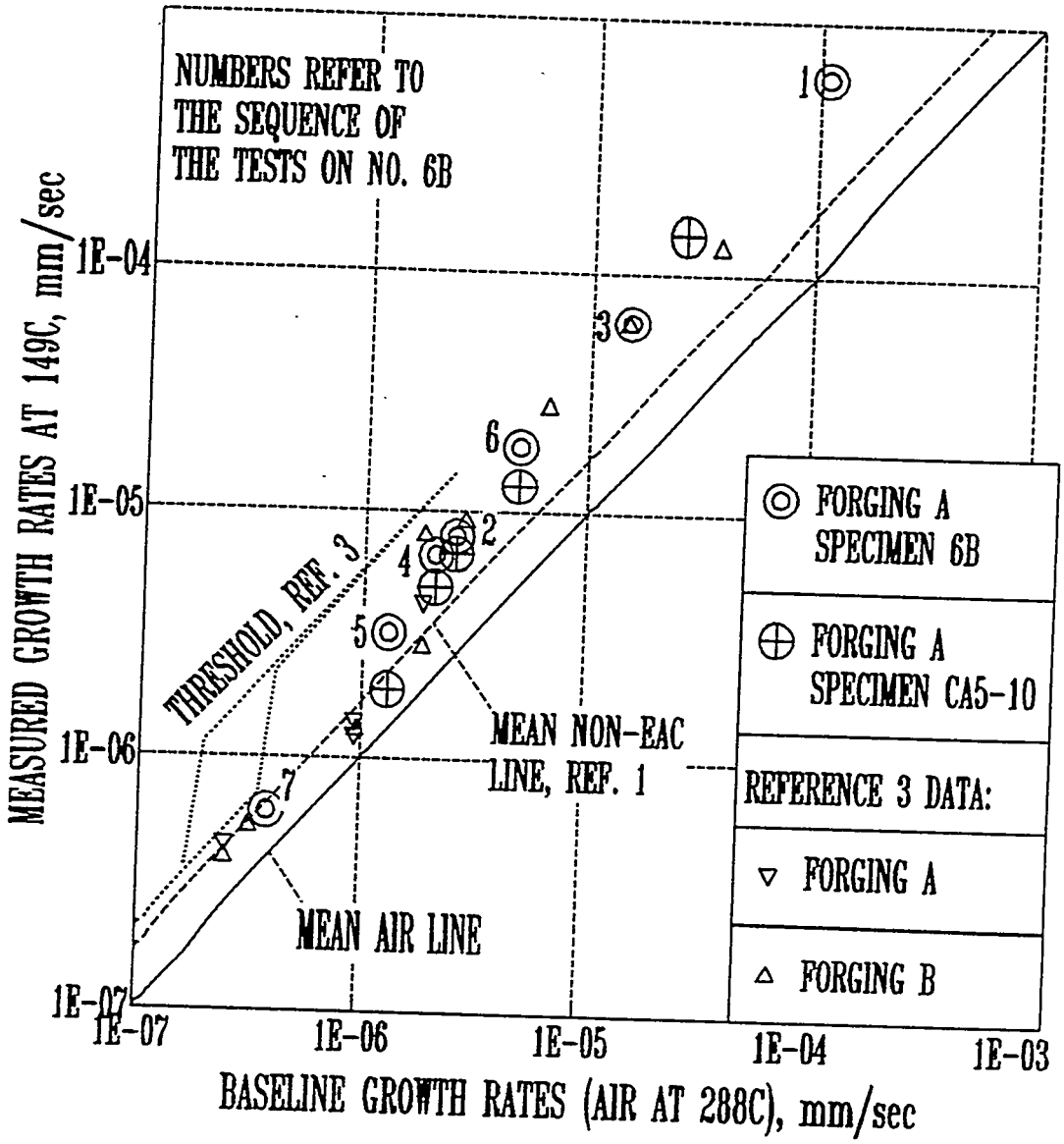

Figure 4. Environmental Fatigue Crack Growth Rates for Forging A at 149°C Plotted Against Baseline Crack Growth Rates. The present data are shown as enlarged symbols.

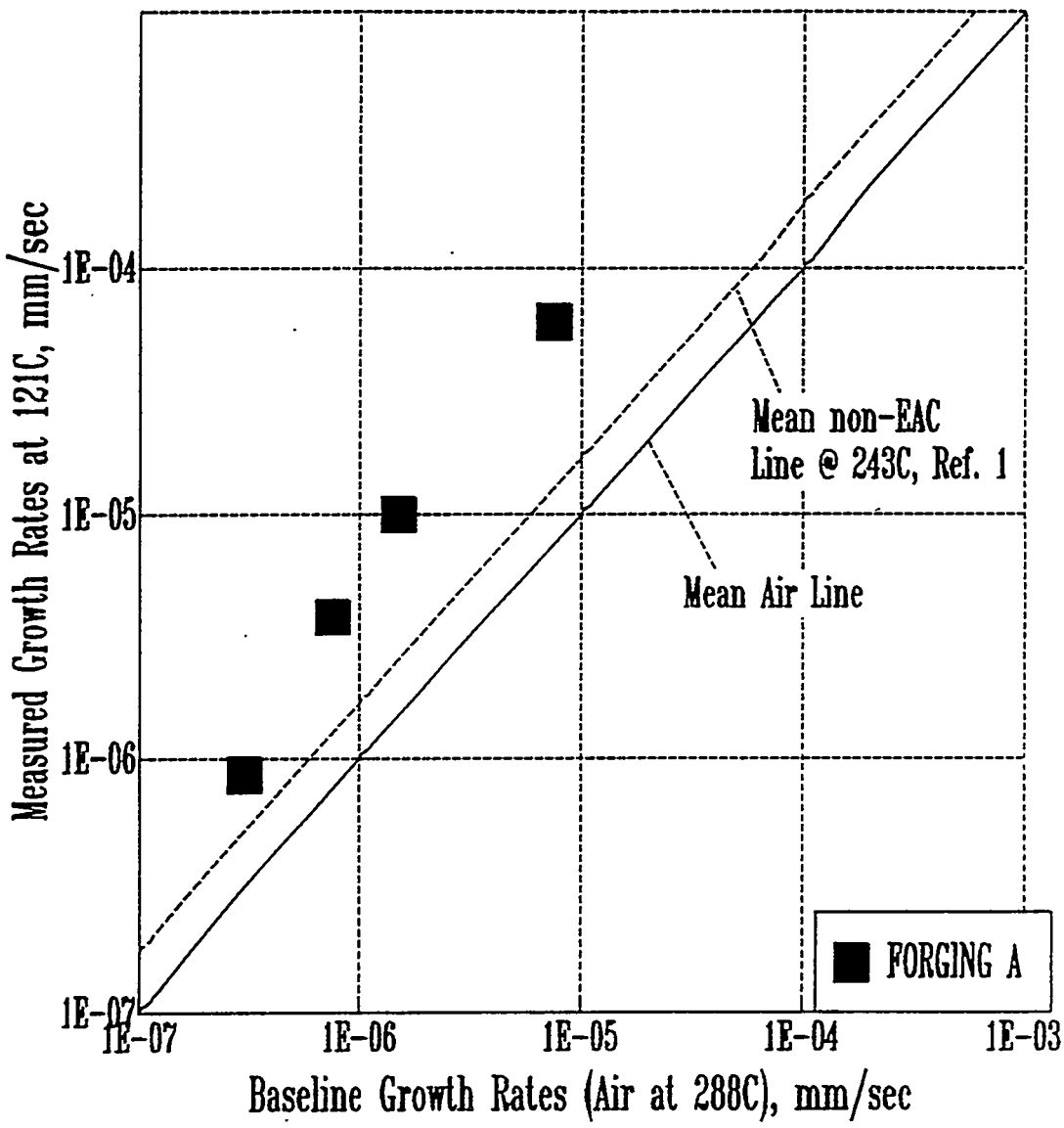

Figure 5. Environmental Fatigue Crack Growth Rates for Forging A at 121°C Plotted Against Baseline Air Crack Growth Rates.

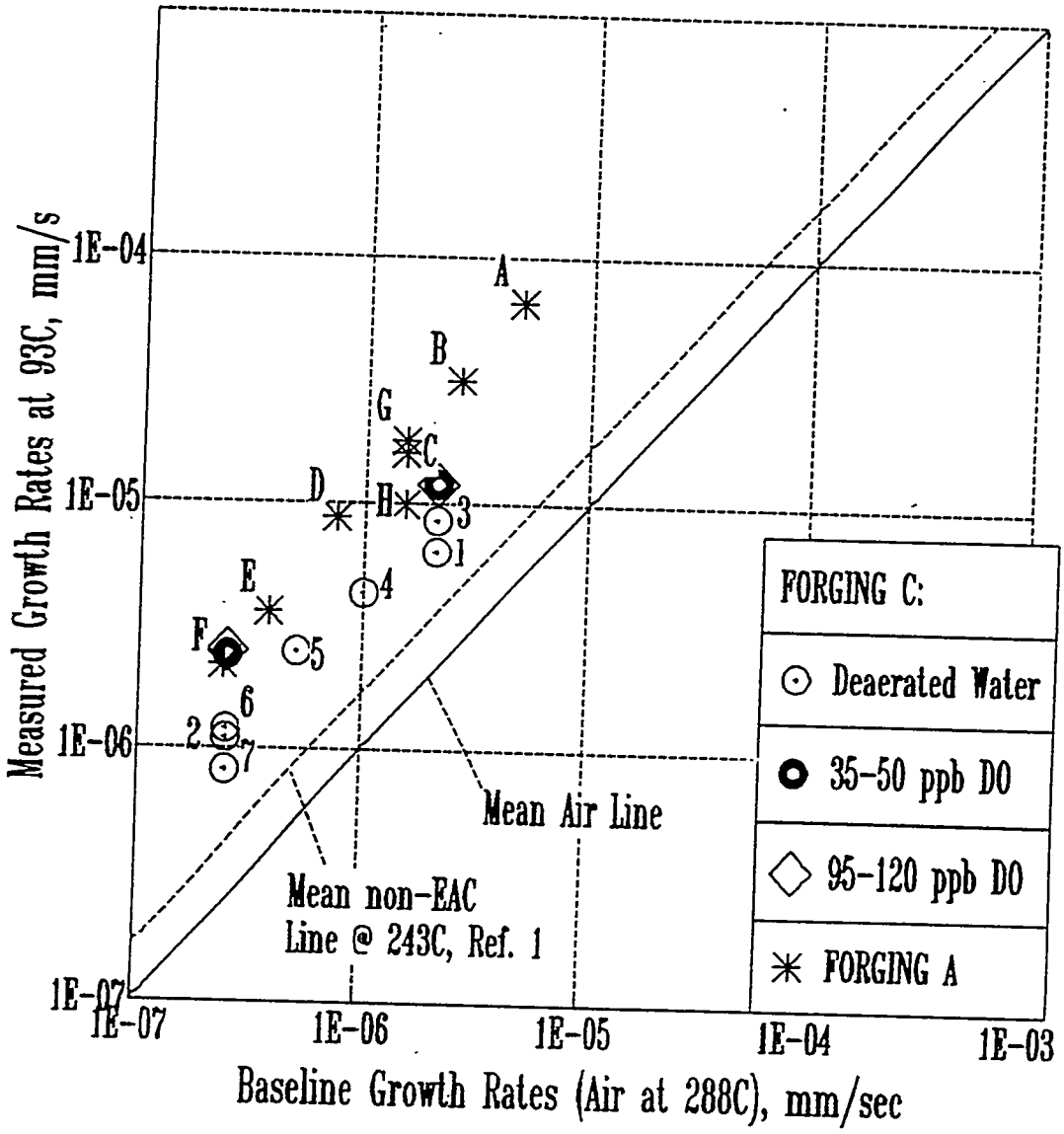

Figure 6. Environmental Fatigue Crack Growth Rates for Forgings A and C at 93°C Plotted Against Baseline Crack Growth Rates. The numbers and letters indicate the sequence of tests on specimens CA5-50 and 6B, respectively.

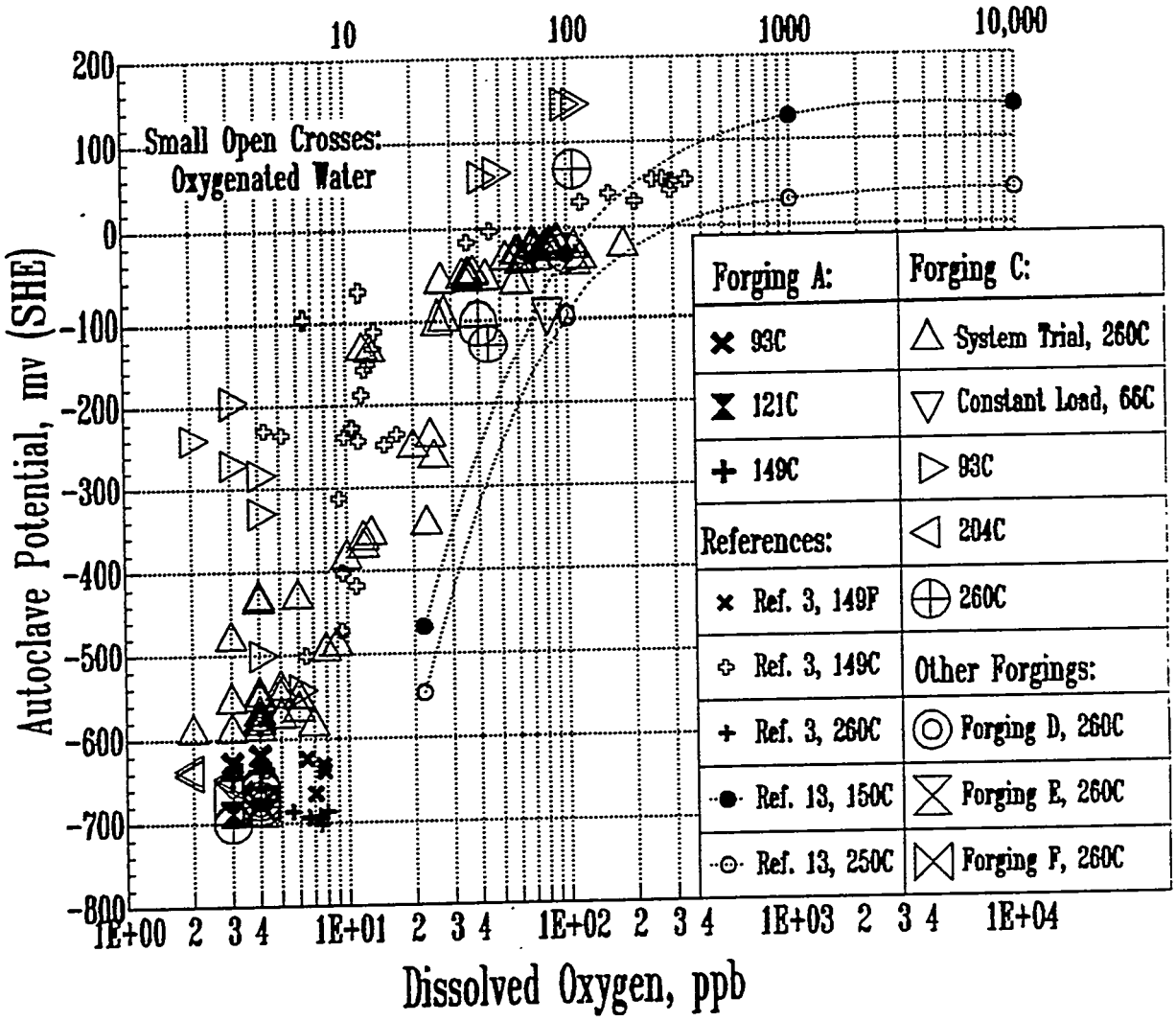

Figure 7. Summary of the Corrosion Potential Data for the Present Tests.

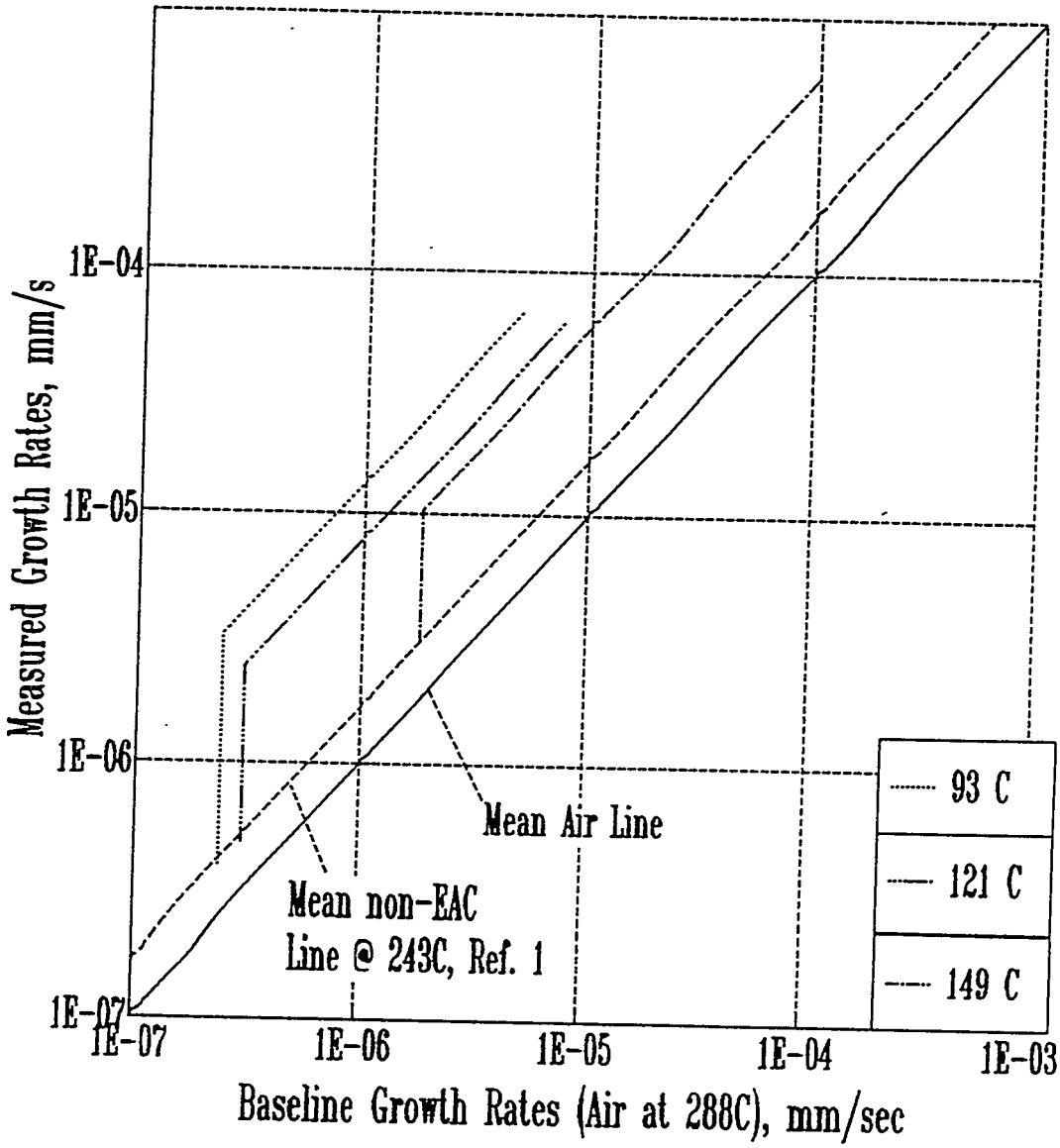

Figure 8. Schematic View of the Effect of Temperature Suggested by the Present Data.

APPENDIX I. INDIVIDUAL TEST CONDITIONS USED IN THE FATIGUE CRACK GROWTH RATE PROGRAM.

Table A-I. Fatigue Crack Growth Rate Data for Forgings D, E, and F at 260°. All tests: ΔK = 16.5 Mpa$\sqrt{m}$, R = 0.7, under low oxygen (≈4 ppb) conditions.

Specimen Number /Forging	Rise Time s	Measured Cyclic Rates mm/cycle	Crack Growth Rates Measured $\dot{a}_E$, mm/s	Crack Growth Rates Baseline $\dot{a}_B$, mm/s	FCGR Ratio $\dot{a}_E/\dot{a}_B$	Comments
CA5-51	19.0	9.2E-5	4.8E-6	2.1E-6	2.3	
/Forging D	158.3	7.0E-5	4.4E-7	2.5E-7	1.8	
CA5-70	19.0	5.8E-5	3.0E-6	2.1E-6	1.5	
/Forging E	158.3	1.1E-4	6.9E-7	2.5E-7	2.8	1500 cycles
		4.6E-5	2.9E-7		1.2	
	4.2	4.3E-5	1.0E-5	9.3E-6	1.1	
CA5-80	19.0	5.9E-5	3.1E-6	2.1E-6	1.5	
/Forging F	158.3	1.2E-4	7.8E-7	2.5E-7	3.1	2000 cycles
		5.9E-5	3.7E-7		1.5	
	4.2	4.7E-5	1.1E-5	9.3E-6	1.2	

Table A-II. Fatigue Crack Growth Rate Data for Forging A at Temperatures ≤149°C under Low Oxygen (≈ 4 ppb) Conditions. Load ratio: R = 0.3 for all tests. ΔK = 40.2 Mpa√m, unless otherwise noted.

Specimen Number	Test Temp. °C	Test s	Rise Time mm/cycle	Measured Cyclic Rates $\dot{a}_E$, mm/s	$\dot{a}_B$, mm/s	Crack Growth Rates Measured $\dot{a}_E/\dot{a}_B$	FCGR Baselin Ratio Notes
6B	149	3.2	1.9E-3	5.9E-4	1.1E-4	5.2	
	149	135.7	1.1E-3	7.9E-6	2.6E-6	3.0	
	149	29.9	1.8E-3	6.1E-5	1.5E-5	4.1	ΔK = 42.9, Sine Wave.
	149	95.0	6.2E-4	6.6E-6	2.1E-6	3.7	ΔK = 33.0.
	149	153.2	4.9E-4	3.2E-6	1.3E-6	2.5	ΔK = 33.0.
	149	73.1	1.4E-3	1.9E-5	4.9E-6	3.8	
	149	950.0	5.7E-4	6.0E-7	3.8E-7	1.6	
CA5-10	149	13.6	2.0E-3	1.4E-4	2.6E-5	5.4	
	149	73.1	9.6E-4	1.3E-5	4.9E-6	2.7	
	149	135.7	9.1E-4	6.7E-6	2.6E-6	2.6	
	149	95.0	4.6E-4	4.9E-6	2.1E-6	2.4	ΔK = 33.0.
	149	153.2	2.8E-4	1.9E-6	1.3E-6	1.5	ΔK = 33.0.
	149	135.7	9.4E-4	6.9E-6	2.6E-6	2.6	
6B	121	237.5	2.5E-3	1.0E-5	1.5E-6	6.9	
	121	47.5	2.9E-3	6.0E-5	7.5E-6	8.0	
	121	475.0	1.8E-3	3.8E-6	7.5E-7	5.0	
	121	1187.5	1.0E-3	8.6E-7	3.0E-7	3.2	
6B	93	73.1	4.1E-3	6.6E-5	4.9E-6	11.4	
	93	135.7	4.3E-3	3.2E-5	2.6E-6	11.9	
	93	237.5	3.9E-3	1.6E-5	1.5E-6	10.9	
	93	475.0	4.2E-3	8.8E-6	7.5E-7	11.6	
	93	950.0	3.5E-3	3.6E-6	3.8E-7	9.7	
	93	1461.5	3.2E-3	2.2E-6	2.4E-7	9.1	
	93	237.5	4.2E-3	1.8E-5	1.5E-6	11.8	
	93	237.5	2.4E-3	1.0E-5	1.5E-6	6.8	Changed autoclave

Table A-III. Fatigue Crack Growth Rate Data for Specimen CA5-50 from Forging C. $\Delta K = 16.5$ Mpa$\sqrt{m}$, R = 0.7.

Test No.	Test Temp. °C	Rise Time s	Measured Cyclic Rates mm/cycle	Crack Growth Rates Measured $\dot{a}_E$, mm/s	Baseline $\dot{a}_B$, mm/s	Ratio $\dot{a}_E/\dot{a}_B$	FCGR Oxygen, ppb	Dissolved Notes
1.	93	19.0	1.2E-4	6.4E-6	2.1E-6	3.1	6	
2.	93	158.3	1.9E-4	1.2E-6	2.5E-7	5.0	4	
3.	260	19.0	1.0E-4	5.5E-6	2.1E-6	2.6	4	
4.	260	158.3	1.1E-4	6.6E-7	2.5E-7	2.7	4	
5.	Exposed for 2 days at 66°C at constant load and 70 to 80 ppb Oxygen.							
6.	260	19.0	8.6E-5	4.6E-6	2.1E-6	2.2	3	
7.	260	158.3	1.1E-4	7.1E-7	2.5E-7	2.9	4	
8.	260	19.0	6.3E-4	3.3E-5	2.1E-6	16.1	33 to 55	
9.	260	158.3	2.5E-3	1.6E-5	2.5E-7	64.3	50 to 29	
10.	93	19.0	2.3E-4	1.2E-5	2.1E-6	5.7	49 to 44	
11.	93	158.3	3.8E-4	2.4E-6	2.5E-7	9.9	44 to 35	
12.	260	19.0	8.9E-4	4.6E-5	2.1E-6	22.6	107	
13.	260	158.3	2.8E-3	1.8E-5	2.5E-7	73.9	107 to 92	
14.	93	19.0	2.4E-4	1.2E-5	2.1E-6	6.1	95 to 94	
15.	93	158.3	4.1E-4	2.5E-6	2.5E-7	10.0	94 to 118	
16.	93	19.0	1.6E-4	8.6E-6	2.1E-6	4.2	4	
17.	93	38.0	1.6E-4	4.3E-6	1.0E-6	4.1	2	
18.	93	76.0	1.8E-4	2.5E-6	5.1E-7	4.6	2	
19.	93	158.3	1.8E-4	1.1E-6	2.5E-7	4.5	3	First 1550 cycles
			1.3E-4	8.3E-7		3.3		Next 4400 cycles
20.	204	19.0	2.3E-4	1.2E-5	2.1E-6	5.9	2	First 3000 cycles
			1.2E-4	6.0E-6		2.9		Next 5000 cycles
21.	204	38.0	7.2E-5	1.9E-6	1.0E-6	1.8	2	
22.	204	76.0	9.2E-5	1.2E-6	5.1E-7	2.4	2	
23.	204	9.5	1.0E-4	1.1E-5	4.1E-6	2.7	3	
24.	204	19.0	7.5E-6	4.0E-6	2.1E-6	1.9	3	